

Escape in Hill's Problem

Douglas C Heggie

University of Edinburgh, UK

1 Introduction and Motivation

In the 19th century the American mathematician G.W. Hill devised a simple and useful approximation for the motion of the moon around the earth with perturbations by the sun. To most dynamical astronomers “Hill’s Problem” still means a model for motions in the solar system in which two nearby bodies move in nearly circular orbits about another much larger body at a great distance. These lectures have, however, been motivated by a problem in stellar dynamics.

Consider a star in a star cluster which is itself in orbit about a galaxy (Figure 2). The star, cluster and galaxy take the place of the moon, earth and sun, respectively. The potentials of the cluster and galaxy are not those of a point mass, and the galactic orbits of the star and cluster may be far from circular. Nevertheless Hill’s problem is a good starting point, and it can be modified easily to accommodate the differences. In section 2 we outline a derivation of Hill’s equations, and in section 3 we summarise the appropriate extensions.

Stars gradually escape from star clusters. This has been expected on theoretical grounds for many years, ever since a paper by Ambartsumian (1938). Recently, deep observations have confirmed this (e.g. Leon et al 2000), by revealing faint streams of stars around a number of the globular clusters of our Galaxy.

Loosely speaking we can say that a star can only escape if its energy exceeds some critical energy. The energies of stars change slightly as a result of two-body gravitational encounters within clusters, though the time scale on which this happens (the *relaxation time scale*) is very long, of order 10^9 yr. But the orbital motions of stars within clusters have much smaller time scales of order 10^6 yr, and until recently it was thought that escaping stars would leave on a similar time scale. With this assumption, relaxation is the bottleneck, and so the escape time scale (e.g. the time taken for half the stars to escape) should vary with the relaxation time.

Nowadays it is possible to simulate the evolution of modest-sized star clusters with 3×10^4 or more members, and the predicted escape time scale can be checked empirically. Unfortunately the results contradict the theory (Figure 1). As these simulations require

considerable extrapolation in particle number N to be applicable to real clusters (for which $N \sim 10^6$) the error of the theory is serious.

It turns out that the assumption of rapid escape is the main source of error (Fukushige & Heggie 2000, Baumgardt 2000a,b). In fact some stars above the escape energy never escape (unless some other dynamical process comes into play), and others take much longer to escape than had been generally thought.

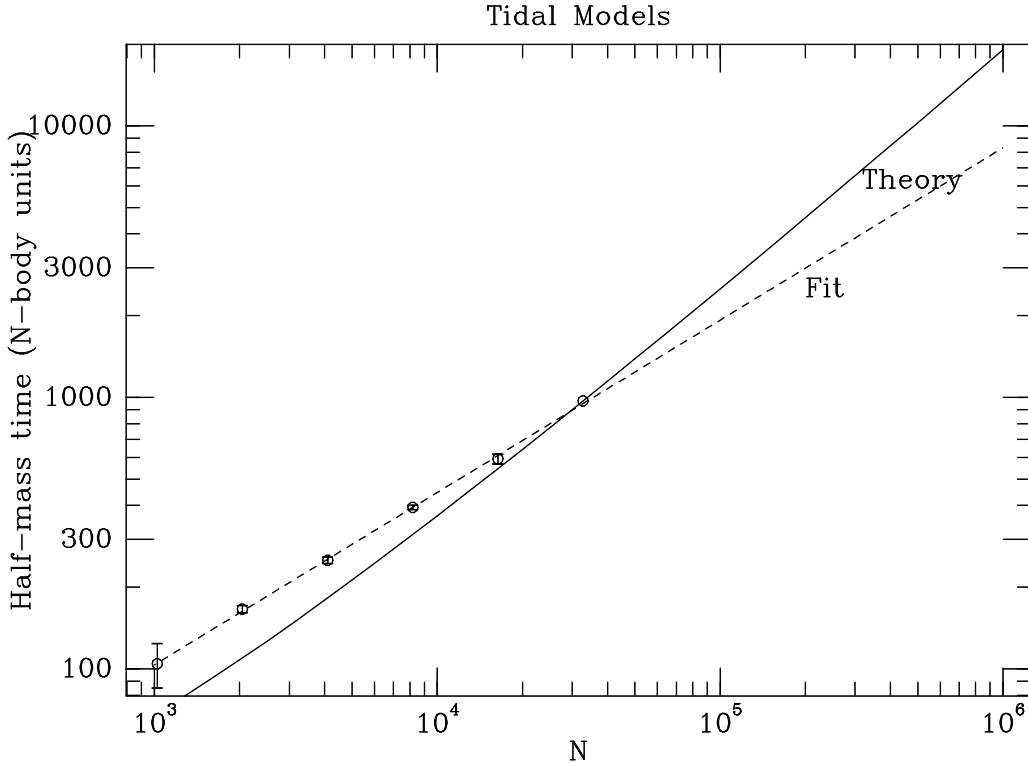


Figure 1. Results of numerical experiments (Aarseth & Heggie, unpublished) on the escape of stars from star clusters. The time for half the stars to escape is plotted against the original number N of stars in the simulation. Points are averages over several simulations at each N , except the largest value. The continuous line shows the prediction of theory, i.e. proportional to the relaxation time (see text), and the dashed line is an empirical fit.

With this motivation, the remaining sections of these lectures are devoted to the dynamics of escape. Section 4 analyses the very definition of escape, which is not as straightforward as in more familiar situations. The last two sections show some ways in which the computation of the escape rate can be approached. The main result of section 5 concerns the way in which the time scale of escape depends on the energy, and outlines how this resolves the problem of Figure 1. Much more difficult, from a theoretical point of view, is determining the *distribution* of escape times, and some relevant ideas are introduced in Section 6.

2 Equations of Motion

2.1 Derivation

We now outline a derivation of the equations of Hill's problem in the stellar dynamics context. To simplify matters as much as possible, however, we treat the cluster and galaxy as point masses M_c and $M_g \gg M_c$ (Figure 2), and consider motion of a massless star in the same plane of motion.

If x, y are the coordinates of the star in a rotating frame centred at the cluster centre, its velocity relative to the galaxy is $(\dot{x} - \omega y, \dot{y} + \omega[R + x])$. Therefore the Lagrangian for its motion is $\mathcal{L} = \frac{1}{2} \{(\dot{x} - \omega y)^2 + (\dot{y} + \omega(R + x))^2\} + \frac{GM_g}{R'} + \frac{GM_c}{r}$, where $r^2 = x^2 + y^2$ and $R'^2 = (R + x)^2 + y^2$. (Note here that we are neglecting the motion of the galaxy, which will not affect the final approximate set of equations of motion.)

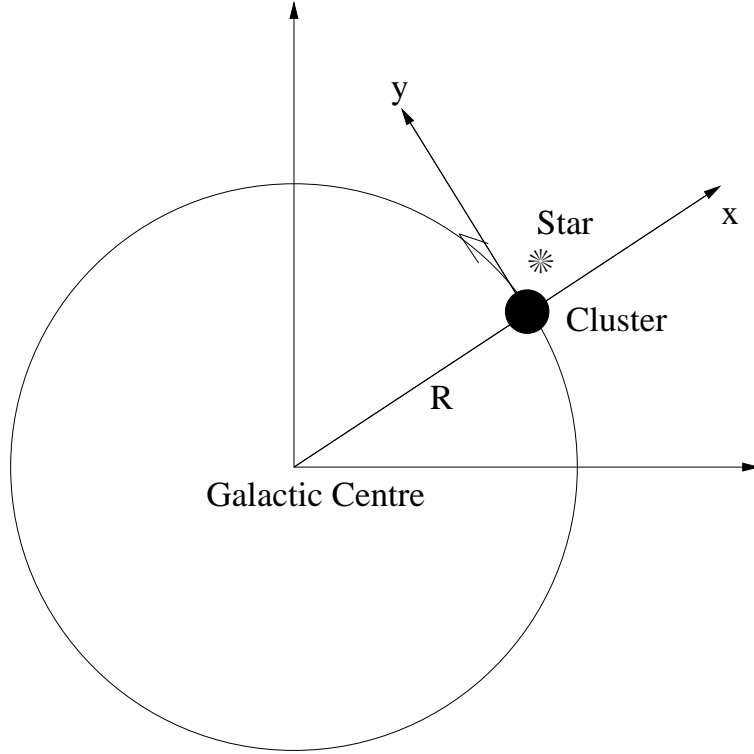


Figure 2. Derivation of Hill's equations. The cluster is treated as a point mass M_c in uniform circular motion of angular velocity ω at a distance R from a point-mass galaxy M_g .

For reasons that will become clear later we switch to a canonical formulation. The momenta conjugate to x and y are

$$\begin{aligned} p_x &= \mathcal{L}_{\dot{x}} = \dot{x} - \omega y \\ p_y &= \mathcal{L}_{\dot{y}} = \dot{y} + \omega(R + x), \end{aligned}$$

and the Hamiltonian is

$$\begin{aligned} \mathcal{H} &= \dot{x}p_x + \dot{y}p_y - \mathcal{L} \\ &= \frac{1}{2}(p_x^2 + p_y^2) + \omega(yp_x - [R + x]p_y) - \frac{GM_g}{R'} - \frac{GM_c}{r}. \end{aligned}$$

The next step is common to applications in the solar system and stellar dynamics but has a different name. In applications to the earth-moon-sun problem it is referred to as “neglect of the parallax”, while in stellar dynamics it is always called a “tidal approximation”. (Even that phrase betrays how much the subject of stellar dynamics owes to the celestial mechanics of the earth-moon-sun system!) We suppose $r \ll R$ and approximate $\frac{1}{R'} \simeq (1 - \frac{x}{R} + \frac{1}{2} \frac{2x^2 - y^2}{R^2})/R$. We drop constant terms, substitute $\omega^2 = GM_g/R^3$ from the equations of circular motion (again assuming $M_c \ll M_g$), and replace $p_y \rightarrow p_y + \omega R$. (If the other variables are not changed this transformation is canonical.) Then we get $\mathcal{H} = \frac{1}{2}(p_x^2 + p_y^2) + \omega(y p_x - x p_y) - \frac{1}{2}\omega^2(2x^2 - y^2) - \frac{GM_c}{r}$.

Next we write down Hamilton’s equations

$$\dot{x} = \mathcal{H}_{p_x}, \dot{p}_x = -\mathcal{H}_x, \quad (1)$$

etc. Finally, on eliminating p_x and p_y , we get

$$\ddot{x} - 2\omega\dot{y} - 3\omega^2 x = -\frac{GM_c}{r^3}x \quad (2)$$

$$\ddot{y} + 2\omega\dot{x} = -\frac{GM_c}{r^3}y, \quad (3)$$

which differ from Hill’s equations only in notation, and then only slightly.

2.2 A Generalised Leapfrog

The leapfrog is a favourite integration algorithm for equations of motion in stellar dynamics. It is identical to the Verlet algorithm of molecular dynamics. For a one-dimensional problem with Hamiltonian $p^2/2 + V(x)$, for example, it *may* be written

$$x_{n+1} = x_n + h p_n \quad (4)$$

$$p_{n+1} = p_n - h V'(x_{n+1}), \quad (5)$$

where h is the time step. Note that the new coordinate is used immediately, which is where the algorithm differs from an Euler algorithm. The effect is dramatic, as the long-term behaviour of the leapfrog is *much* better.

One of the nice properties of the leapfrog is that it is *symplectic*, like a good Hamiltonian flow. Here we show how to construct a similar algorithm for the Hamiltonian of Hill’s problem.

Euler’s algorithm would be

$$\mathbf{x}_{n+1} = \mathbf{x}_n + h \mathcal{H}_{\mathbf{p}}(\mathbf{x}_n, \mathbf{p}_n), \mathbf{p}_{n+1} = \mathbf{p}_n - h \mathcal{H}_{\mathbf{x}}(\mathbf{x}_n, \mathbf{p}_n),$$

where we have written $\mathbf{x} = (x, y)$ and $\mathbf{p} = (p_x, p_y)$. We can make this symplectic by replacing \mathbf{p}_n by \mathbf{p}_{n+1} in the arguments of the derivatives of \mathcal{H} , because it then takes the form

$$\mathbf{x}_{n+1} = \mathcal{F}_{\mathbf{p}}(\mathbf{x}_n, \mathbf{p}_{n+1}), \mathbf{p}_n = \mathcal{F}_{\mathbf{x}}(\mathbf{x}_n, \mathbf{p}_{n+1}),$$

where the generating function $\mathcal{F} = \mathbf{x}_n \cdot \mathbf{p}_{n+1} + h \mathcal{H}(\mathbf{x}_n, \mathbf{p}_{n+1})$.

Writing out these equations explicitly for the Hamiltonian of Hill's problem, we obtain the algorithm

$$x_{n+1} = x_n + h(p_{x,n+1} + \omega y_n) \quad (6)$$

$$y_{n+1} = y_n + h(p_{y,n+1} - \omega x_n) \quad (7)$$

$$p_{x,n} = p_{x,n+1} + h(-\omega p_{y,n+1} - 2\omega^2 x_n + \frac{GM_c}{r_n^3} x_n) \quad (8)$$

$$p_{y,n} = p_{y,n+1} + h(\omega p_{x,n+1} + \omega^2 y_n + \frac{GM_c}{r_n^3} y_n). \quad (9)$$

These equations look horribly implicit, a common difficulty with elementary derivations of symplectic methods, but in fact eqs.(8) and (9) are easily solved explicitly for \mathbf{p}_{n+1} and then eqs.(6) and (7) give \mathbf{x}_{n+1} .

2.3 Elementary Properties

1. The Hamiltonian \mathcal{H} is time-independent, and so its value is conserved. Rewriting the momenta in terms of the velocity components one finds that this value is $E = \frac{1}{2}(\dot{x}^2 + \dot{y}^2) - \frac{3}{2}\omega^2 x^2 - \frac{GM_c}{r}$, which is often referred to as the “energy”. Again there is another name in the celestial mechanics community, who refer to the “Jacobi constant” $C = -2E$. In stellar dynamics this term is often applied to E . At any rate, one implication is that the motion is bounded to the region in which $-\frac{3}{2}\omega^2 x^2 - \frac{GM_c}{r} \leq E$. The boundaries of these regions are called *Hill's curves* (Figure 3).

It is sometimes tempting to refer to the expression for E as the Hamiltonian, and indeed the right-hand side has the same value as \mathcal{H} . It is, however, impossible to recover the equations of motion from the expression for E .

2. Hill's equations have two equilibrium solutions, at $(x, y) = \pm(r_t, 0)$, where $r_t^3 = GM_c/(3\omega^2)$. In stellar dynamics r_t is called the *tidal radius* or *Jacobi radius*, and in all subjects these points are referred to as the *Lagrange points* L_1 and L_2 .
3. Hill's equations have an obvious symmetry: if $(x(t), y(t))$ is a solution, then so is $(x'(t), y'(t)) = (x(-t), -y(-t))$. This is quite useful for studying *asymptotic* orbits. For example, if an orbit tends to L_1 as $t \rightarrow \infty$, then the orbit obtained by this symmetry tends to L_1 as $t \rightarrow -\infty$. Also, if $\dot{x}(0) = y(0) = 0$, the two orbits are the same, as they satisfy the same initial conditions. This helps to explain the amount of attention that has been paid in the literature to such orbits.

3 Variants of the Problem

1. It is not necessary that one of the bodies is massless. Hill's equations are also applicable to the relative motion of the moon and earth, under solar perturbation, as in Hill's original research. A relatively accessible account of this research is Plummer (1918). A modern application is binary asteroids (e.g. Chauvineau & Mignard 1990).

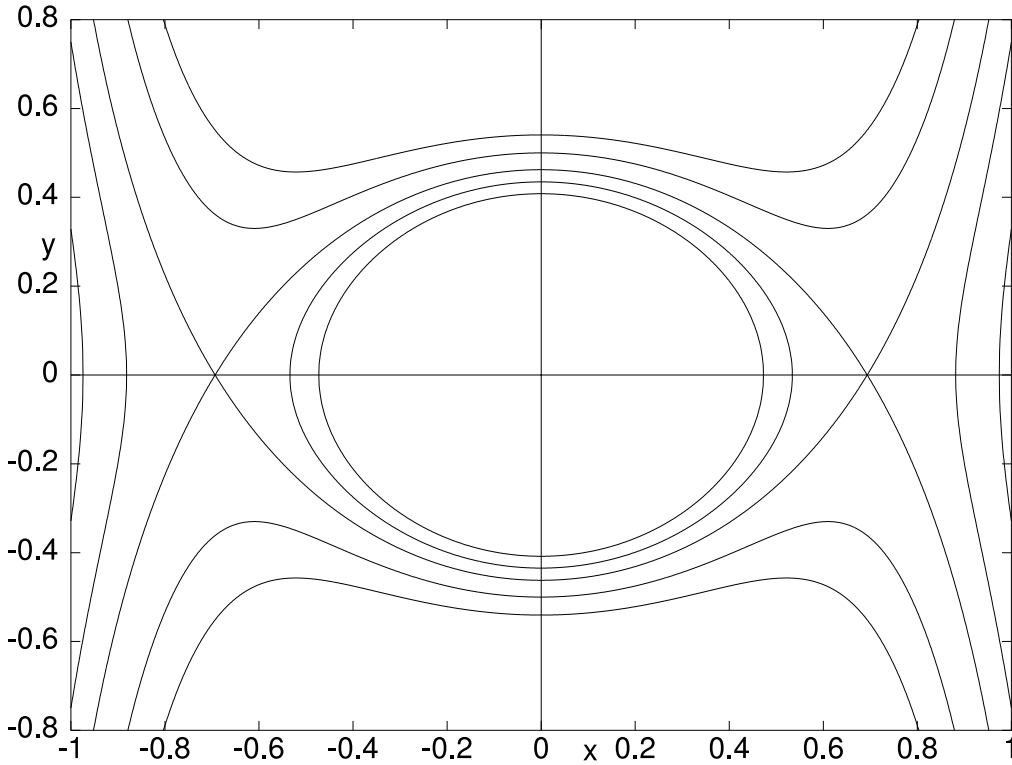


Figure 3. Hill's curves.

2. It is not necessary that the two small bodies are bound. Another application is to near-conjunctions of coorbital (e.g. Murray & Dermott 1999).
3. When the smallest body is treated as massless, as in the star cluster application, it is not necessary that the other bodies are treated as point masses. For a spherically symmetric galaxy potential and an arbitrary cluster potential ϕ_c the three-dimensional equations of motion are

$$\begin{aligned}\ddot{x} - 2\omega\dot{y} + (\kappa^2 - 4\omega^2)x &= -\frac{\partial\phi_c}{\partial x} \\ \ddot{y} + 2\omega\dot{x} &= -\frac{\partial\phi_c}{\partial y} \\ \ddot{z} + \omega^2z &= -\frac{\partial\phi_c}{\partial z}\end{aligned}$$

where κ is the *epicyclic frequency* (Chandrasekhar 1942, Binney & Tremaine 1987) and the plane of motion of the cluster is the x, y plane. For a point-mass galaxy $\kappa = \omega$ and the previous equations are recovered (when $\phi_c = -GM_c/r$.)

Very often the cluster potential ϕ_c would be chosen to be that of a *King model* (cf. Binney & Tremaine 1987). Qualitatively the most important difference from the point-mass potential is that the depth of the potential well is finite. Figure 5 illustrates the differences which a change of potential can make.

4. Returning to the point mass case, we now consider the situation in which the motion of the cluster is elliptic, with eccentricity e . There is now a formulation using the same coordinates as in Figure 2 but scaled by R (so-called *rotating, pulsating*

coordinates \tilde{x}, \tilde{y}). For coplanar motion the equations are

$$\begin{aligned}\tilde{x}'' - 2\tilde{y}' &= \frac{1}{1+e \cos f} \left(3\tilde{x} - \frac{M_c}{M_g} \frac{\tilde{x}}{\tilde{r}^3} \right) \\ \tilde{y}'' + 2\tilde{y}' &= \frac{1}{1+e \cos f} \left(-\frac{M_c}{M_g} \frac{\tilde{y}}{\tilde{r}^3} \right),\end{aligned}$$

where ' denotes differentiation with respect to f , the true anomaly of the cluster orbit, and $\tilde{r}^2 = \tilde{x}^2 + \tilde{y}^2$. These equations can be easily derived from the corresponding formulation of the elliptic restricted problem (Szebehely 1967). An important difference from the circular case is that the Hamiltonian is no longer autonomous, and there is no Jacobi integral.

5. One can equally well treat the previous problem in rotating, *non*-pulsating coordinates with origin at the centre of the cluster. For coplanar motion, a point-mass galaxy and an arbitrary cluster potential, the equations are

$$\begin{aligned}\ddot{x} - 2\omega\dot{y} - (3\omega^2 - 2\frac{\ddot{R}}{R})x + 2\omega\frac{\dot{R}}{R}y &= -\frac{\partial\phi_c}{\partial x} \\ \ddot{y} + 2\omega\dot{x} - \frac{\ddot{R}}{R}y &= -\frac{\partial\phi_c}{\partial y},\end{aligned}$$

but the corresponding three-dimensional equations can easily be derived for any spherical galaxy potential (Oh, Lin & Aarseth 1992). Here, of course, ω is not constant in general.

6. For a still more general galaxy potential ϕ_g it is simplest to use non-rotating, non-pulsating coordinates, i.e. a coordinate frame with origin at the cluster centre but with axes parallel to fixed directions in space. Then the equation of motion takes the simple vector form $\ddot{\mathbf{r}} = -\nabla\phi_c - \mathbf{r} \cdot \nabla\nabla\phi_g$.

Though this may well be the most useful formulation for non-circular cluster motion, and certainly when the potential is not even spherical, one can't help feeling that something is lost in this simplicity. For example, in the case of a point mass galaxy the equation of motion is

$$\ddot{\mathbf{r}} = -\nabla\phi_c - \omega^2(\mathbf{r} - 3(\mathbf{r} \cdot \hat{\mathbf{R}})\hat{\mathbf{R}}), \quad (10)$$

where $\hat{\mathbf{R}}$ is the unit vector from the galaxy to the cluster. Now the corresponding Hamiltonian is time-dependent, and it is no longer obvious that any integral exists. But the Jacobi integral is still conserved, taking the form

$$E = \frac{1}{2}\dot{\mathbf{r}}^2 - \boldsymbol{\omega} \cdot \mathbf{r} \times \dot{\mathbf{r}} + \frac{1}{2}\omega^2 r^2 - \frac{3}{2}\omega^2(\mathbf{r} \cdot \hat{\mathbf{R}})^2 + \phi_c.$$

This is an integral of eq.(10), but not quite an obvious one.

4 Escape Criteria

4.1 Escapers

An escaping star eventually travels far from the cluster, and the cluster potential is negligible. If the right sides of eqs.(2) and (3) are neglected we have the approximate solution

$$x = X + a \cos(t + \phi) \quad (11)$$

$$y = Y_0 - \frac{3}{2}Xt - 2a \sin(t + \phi), \quad (12)$$

where X , Y_0 , a and ϕ are constants, and we have scaled t so that $\omega = 1$. Typical orbits are shown in Figure 4, even in places where the cluster potential would not be negligible.

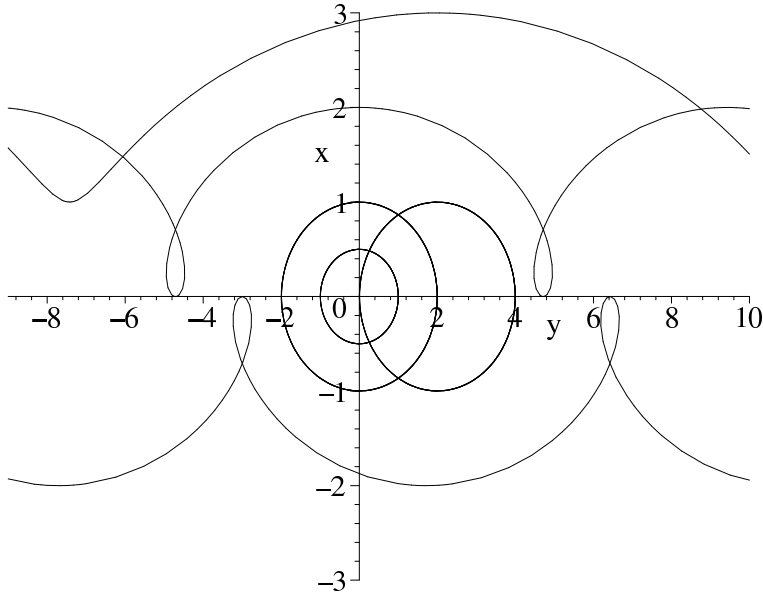


Figure 4. *Orbits in Hill's problem when the cluster potential is neglected. Note that the axes are orientated unconventionally.*

Notice that stars like to revolve or spiral anticlockwise, while the axes are such (Figure 2) that the galaxy is far away at the bottom and the direction of motion of the cluster is to the right. Thus the stellar motions are *retrograde*. This is typical of *epicycles*, as these motions are often called.

Two orbits drawn in Figure 4 are centred at the location of the cluster. There is a family of such orbits, for varying a . When the cluster potential is restored this family becomes a family of stable retrograde satellites of the cluster. Its existence has been known for a long time (Jackson 1913, Hénon 1969, Benest 1971, Markellos 2000). (In the solar system context these are sometimes referred to as *eccentric retrograde satellites*, but the reference to the heliocentric eccentricity is not illuminating in the stellar dynamical context.) This family, referred to as Family f by Hénon, ranges from tiny, almost Keplerian orbits around the origin to huge orbits far beyond the tidal radius. As a star cluster loses mass by the escape of stars, it is conceivable that some stars in retrograde orbits are left on such orbits well outside the tidal radius, and it would be interesting to look for these in N -body simulations.

Now consider the orbit in Figure 4 passing through the origin. Again such orbits of arbitrary size exist (Ross et al 1997). Though severely distorted by the cluster potential

near the origin, they show that stars can escape, recede to arbitrary distance, and then return to the cluster again. Thus distance by itself is no guarantee that escape is permanent. Rigorous escape criteria can be derived, but, to be frank, in practical terms it is quite enough to assume that stars that recede to a few times r_t will escape; the fraction of such stars that do not escape is tiny.

4.2 Non-escapers

It is easy to obtain a rigorous criterion for non-escape, using the simple idea behind Figure 3. A particle at rest at the $L_{1,2}$ points has energy $E_c = -\frac{3}{2} \frac{GM_c}{r_t}$, and any star with $E \leq E_c$, and lying within the Hill curve passing through the Lagrangian points, can never escape.

What now if $E > E_c$? We already know one set of orbits on which a star can remain inside the cluster forever, even with energy above the escape energy: these are the stable retrograde satellites (which move outside the tidal radius only for energies considerably above E_c).

Being stable, these orbits are surrounded by a region of phase space with the same properties. This is illustrated by the surfaces of section in Figure 5. Closed invariant curves predominate on the left side of the diagrams, which corresponds to retrograde motions. At the centre of this nested set of curves is a fixed point corresponding to the retrograde periodic orbit. Though these diagrams are plotted for energy $E = E_c$, similar sets of invariant curves are obtained at somewhat higher energies in the standard Hill problem (Chauvineau & Mignard 1991, Simó & Stuchi 2000). They correspond to retrograde motions of stars permanently remaining inside the cluster and with energies above the energy of escape. The chaotic scattering of points on the right-hand half of the diagram would, however, generally correspond to escaping orbits for $E > E_c$.

It is just possible that such orbits have an astrophysical relevance. In two star clusters (Gunn & Griffin 1979, Meylan et al 1991) there are stars whose *radial* velocity alone appears to exceed the escape velocity. Perhaps these are indeed stars permanently bound within the cluster at energies above the escape energy.

5 Escape Rate

5.1 Motion near the Lagrangian points

Before attempting to determine the rate at which stars escape, we study orbits in Hill's problem a little longer. It is clear from the structure of Hill's curves (Figure 3) that, at energies just above the energy of escape, an escaper must make its way at relatively low speed through one of the gaps in the Hill curves near L_1 and L_2 . Therefore it pays to study motions near these points, which can be done by linearisation of the equations of motion.

In the vicinity of $(x, y) = (r_t, 0)$, when $\omega = GM_c = 1$, eqs.(2) and (3) take the

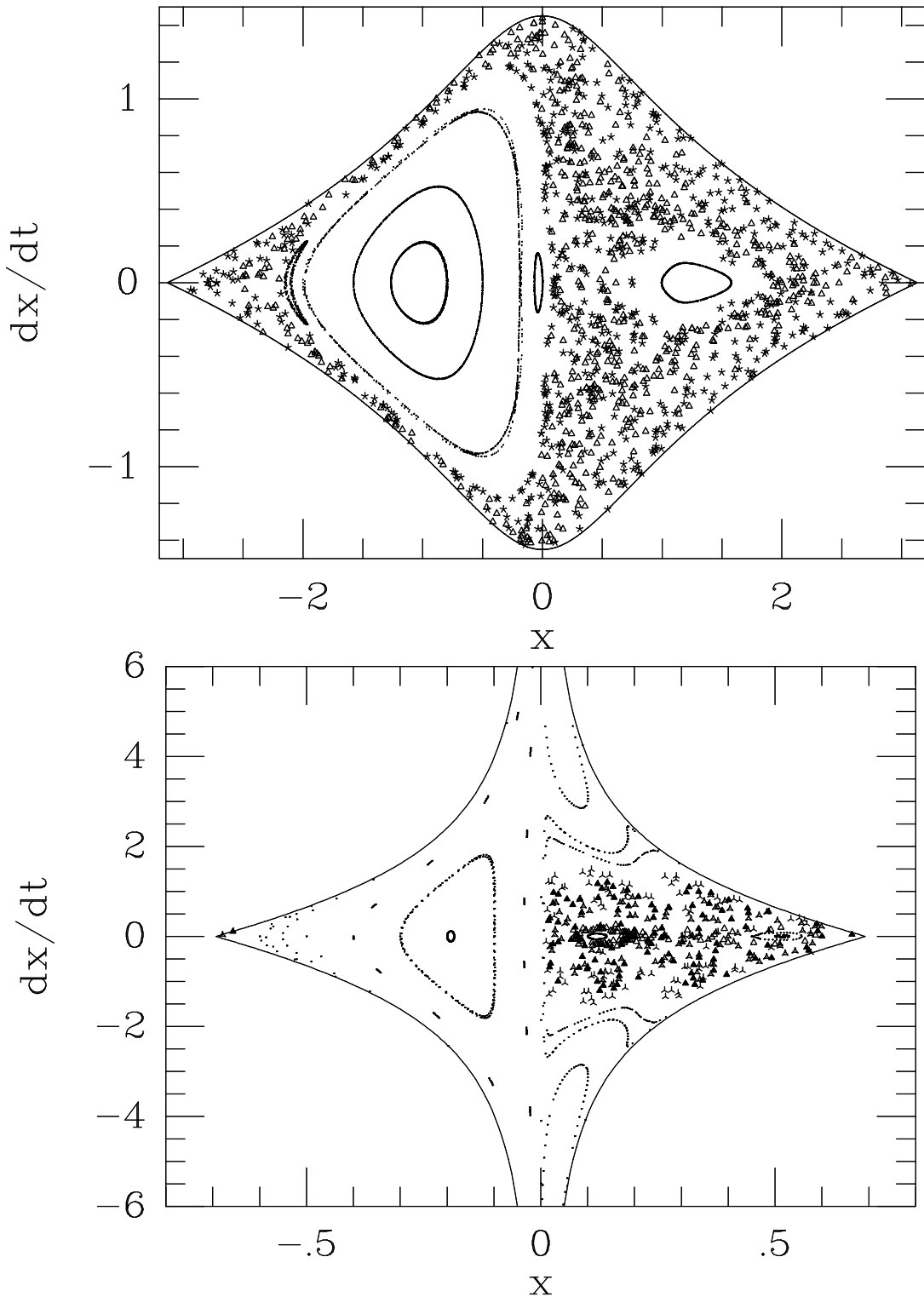


Figure 5. Surface of section in the two-dimensional Hill's problem at the escape energy $E = E_c$. A point is generated on the surface each time an orbit crosses the line $y = 0$ with $\dot{y} > 0$. The edges of the diagram are limiting curves corresponding to the condition $\dot{y} = 0$. Upper diagram: the potential is that of a model star cluster called a King model (from Fukushige & Heggie 2000). Lower diagram: point-mass potential.

approximate form

$$\begin{aligned}\ddot{\xi} - 2\dot{\eta} - 9\xi &= 0 \\ \ddot{\eta} + 2\dot{\xi} + 3\eta &= 0,\end{aligned}$$

where $x = r_t + \xi$ and $y = \eta$. These have the general solution

$$\begin{pmatrix} \xi \\ \eta \end{pmatrix} = A \begin{pmatrix} -\mu \\ 4 - \sqrt{7} \end{pmatrix} \exp(\mu t) + B \begin{pmatrix} \mu \\ 4 - \sqrt{7} \end{pmatrix} \exp(-\mu t) + C \begin{pmatrix} -\nu \cos(\nu t + \theta) \\ (4 + \sqrt{7}) \sin(\nu t + \theta) \end{pmatrix}, \quad (13)$$

where A , B , C and θ are arbitrary constants. On this solution the “energy” is $E = E_c + C^2(10\sqrt{7} + 49) + AB(196 - 40\sqrt{7})$. Several cases have interesting properties:

1. $A = B = C = 0$: this is the Lagrange point, where $E = E_c$ ($\equiv -\frac{3GM_c}{2r_t}$ in general).
2. $B = C = 0$: this solution approaches L_1 as $t \rightarrow -\infty$. It is part of the local unstable invariant manifold of L_1 , and $E = E_c$.
3. $A = C = 0$: this solution approaches L_1 as $t \rightarrow \infty$. It is part of the local stable invariant manifold of L_1 , and $E = E_c$.
4. $A = B = 0$: the solution is periodic, and $E > E_c$. Though derived in a linear approximation, there is indeed a family of periodic solutions of the full Hill problem, parametrised by E (Liapounov's Theorem, cf. Moser 1968). They are named Family a and c (one for each Lagrangian point) in Hénon (1969).
5. $A = 0$: part of the local stable invariant manifold of the Liapounov orbit (Figure 6).
6. $B = 0$: part of the local unstable invariant manifold of the Liapounov orbit.

5.2 The flux of escapers

Stars escaping from the interior of the star cluster have $A < 0$ and $B < 0$, so that $\xi \rightarrow \pm\infty$ as $t \rightarrow \pm\infty$; thus $C^2(10\sqrt{7} + 49) < E - E_c$. For fixed $E > E_c$, then, this is stars “inside” the tube formed by the stable invariant manifold of the Lagrange point (Figure 6). It is quite easy to estimate the rate at which the phase space occupied by these escapers flows out of the cluster. The general theory is given by MacKay (1990), though some trivial generalisation is needed because of the Coriolis forces in Hill's problem.

The rate of flow of phase space (per unit energy E_0) is

$$\mathcal{F} = \int_{\dot{x} > 0, x = r_t} \dot{x} \delta(E(x, y, p_x, p_y) - E_0) dy dp_x dp_y, \quad (14)$$

where the δ -function singles out values of the phase-space variables x, y, p_x, p_y corresponding to the required energy. This is readily transformed to

$$\mathcal{F} = \int_{\dot{\xi} > 0, \xi = 0} \dot{\xi} \delta(E(\xi, \eta, \dot{\xi}, \dot{\eta}) - E_0) d\eta d\dot{\xi} d\dot{\eta} \quad (15)$$

in the notation of Section 5.1. In fact $E = \frac{1}{2}\dot{\xi}^2 + \frac{1}{2}\dot{\eta}^2 - \frac{9}{2}\xi^2 + \frac{3}{2}\eta^2 + E_c$, and so

$$\begin{aligned}\mathcal{F} &= \int_{\frac{1}{2}\dot{\eta}^2 + \frac{3}{2}\eta^2 \leq E_0 - E_c} d\eta d\dot{\eta}, \\ &= \frac{2\pi}{\sqrt{3}}(E_0 - E_c).\end{aligned}$$

This is a two-dimensional result (i.e. for the coplanar problem). In the three-dimensional problem it is found that $\mathcal{F} \propto (E_0 - E_c)^2$, with an equally simple coefficient. In each case, however, the flux of escaping phase space must be doubled, as there are two Lagrangian points.

In order to turn the flux into a time scale for escape, it is only necessary to estimate the volume of phase space inside the cluster at energy E . In turn this is given by an integral of the form $\mathcal{V} = \int_{r < r_t} \delta(E - E_0) dx dy dp_x dp_y$ in two dimensions. This does not change much with E_0 in the vicinity of the critical energy, and there it is easily seen to be 2π times the area inside the last closed Hill curve (Figure 3).

It follows that the time for escape varies as $(E - E_c)^{-2}$ in the three-dimensional problem, though this concerns the dimensionless case in which $\omega = 1$. When dimensional factors are reinserted it turns out that the result is a time scale proportional to $\frac{E_c^2}{(E - E_c)^2 \omega} \frac{1}{\omega}$. This is a central result of these lectures.

5.3 Numerical Methods

It is not hard to obtain the rate of escape numerically. One possible procedure is the following.

1. Choose some $E > E_c$;
2. Select initial conditions at energy E inside the sphere $r = r_t$, according to some distribution (cf. Fukushige & Heggie 2000);
3. Determine the escape time t_e , defined to be the first time when $r > r_t$ (pacé the problem mentioned in Section 4.1);
4. Repeat 2–3 many times;
5. Compute $P(t)$, defined to be the fraction of cases with $t_e > t$.

The third item in this procedure requires choice of a numerical integration scheme. Many are available, but it is worth mentioning here one of the favourites in this subject, which is a fourth-order Hermite scheme (cf. Makino & Aarseth 1992). It is a self-starting scheme, and we illustrate it for the one-dimensional equation of motion $\ddot{x} = a(x)$. Suppose position and velocity are known at the beginning of a time step of length Δt , and have values x_0, v_0 , respectively. From the equation of motion compute the initial acceleration and its initial rate of change, i.e. a_0 and \dot{a}_0 , respectively. Compute the predicted position

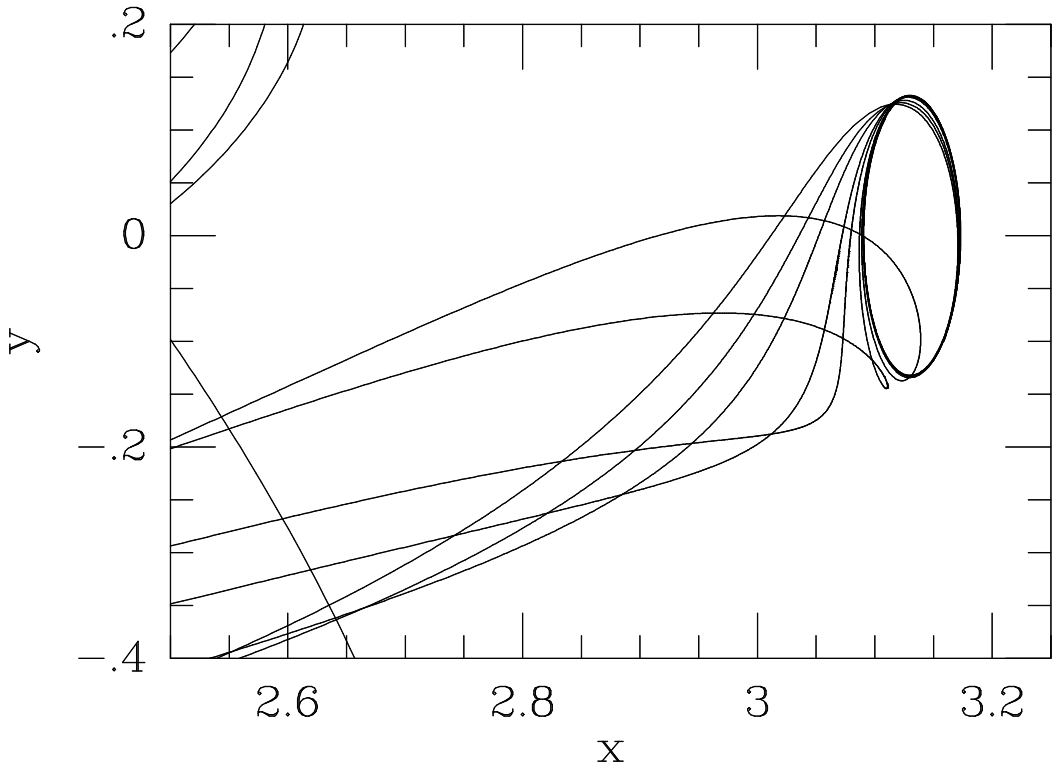


Figure 6. Orbits in Hill's problem around one of the Lagrangian points, at a fixed energy E just above E_c , after Fukushige & Heggie (2000). The potential of the cluster is that of a King model. Several orbits are shown which approach a periodic orbit asymptotically. Other similar diagrams (for the point mass potential of the usual Hill problem) are given in Marchal (1990) and Simó & Stuchi (2000).

and velocity at the end of the time step by

$$\begin{aligned} x_p &= x_0 + v_0 \Delta t + a_0 \frac{\Delta t^2}{2} + \dot{a}_0 \frac{\Delta t^3}{6} \\ v_p &= v_0 + a_0 \Delta t + \dot{a}_0 \frac{\Delta t^2}{2}. \end{aligned}$$

Now compute the acceleration and its derivative at the end of the time step, using x_p and v_p . If the results are denoted by a_1 and \dot{a}_1 , respectively, the values of x and v at the end of the time step are recomputed by

$$\begin{aligned} x_1 &= x_0 + \frac{\Delta t}{2}(v_0 + v_1) - \frac{\Delta t^2}{12}(a_1 - a_0) \\ v_1 &= v_0 + \frac{\Delta t}{2}(a_0 + a_1) - \frac{\Delta t^2}{12}(\dot{a}_1 - \dot{a}_0). \end{aligned}$$

Now we return to the numerical problem of determining the escape rate. A typical set of results is shown in Figure 7. Curves at larger t correspond to smaller values of $E - E_c$. It can be seen that these have a horizontal asymptote well above the t -axis; in other words, there is a substantial fraction of stars for which the escape time is extremely long. This is not unexpected, because of the stable retrograde motions shown in Figure 5. The fraction of such stars decreases as E increases. We also see, as expected from

Section 5.2, that the escape times decrease as E increases. Indeed, if we redefine $P(t)$ to be the fraction of escapers with escape times $t_e > t$ (i.e. we exclude stars which never escape), and if we rescale the values of t by $(E - E_c)^2$, the resulting curves lie very nearly together, independent of energy (Fukushige & Heggie 2000).

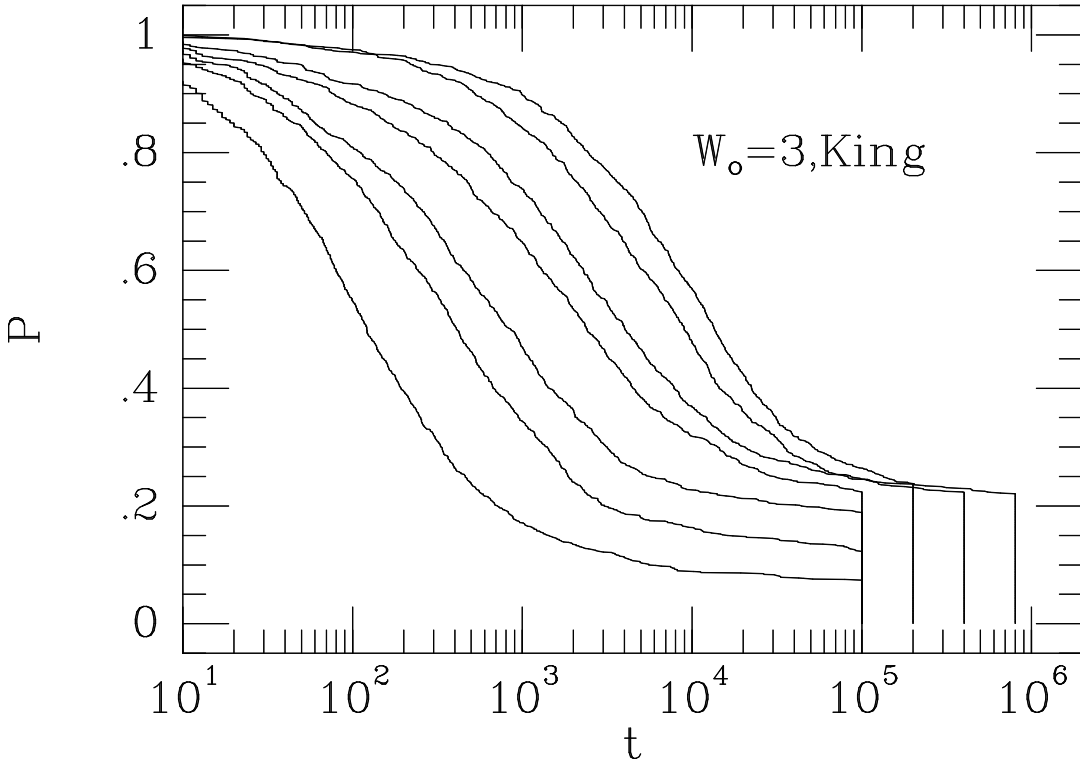


Figure 7. Distribution of escape times from a generalised Hill's problem, for various values of the energy, after Fukushige & Heggie (2000).

5.4 Relaxation and Escape

In this subsection we now show how the escape rate which we have just determined leads to a resolution of the problems with the scaling of N -body simulations, with which these lectures were motivated (Figure 1). The ideas are based on those given in Baumgardt (2000b).

We imagine that stars are present in a cluster with a distribution of energies $n(E)$. This distribution evolves as a result of two processes: (i) relaxation, which is a kind of diffusion process with a characteristic time scale t_r ; and (ii) escape, which takes place on a time scale of order $P\left(\frac{E_c}{E - E_c}\right)^2$, where P is the orbital period of the cluster round the galaxy.

As a very simple model for this problem we shall consider the toy model defined by the differential equation

$$\frac{\partial n}{\partial t} = \frac{E_c^2}{t_r} \frac{\partial^2 n}{\partial E^2} - H(E - E_c) \frac{1}{P} \left(\frac{E - E_c}{E_c}\right)^2 n, \quad (16)$$

where $n(E)dE$ is the number of stars with energies in the range $(E, E + dE)$, and the Heaviside (unit step) function H confines escape to energies above E_c .

There are several details missing from this problem. First, in addition to the diffusive term (i.e. the first term on the right side) one needs a “drift” term corresponding to dynamical friction (cf. Spitzer 1987, for this and other issues in what follows). We have also neglected the fact that the coefficient of the diffusion term depends on E and $n(E)$ in a complicated way. Next, one needs to take into account the effect on the energies of the stars of the slowly changing gravitational potential of the cluster. Finally, we need to take into account the stars above the escape energy whose escape time scale appears to be infinite. If all those factors were included, we would obtain something close to a full Fokker-Planck equation for the evolution of the distribution function in the presence of energy-dependent escape. We shall see, however, that this toy model is quite illuminating.

Let us now scale t by t_r and let $x = (E - E_c)/|E_c|$. Then the escape boundary occurs at $x = 0$, and the equation transforms to

$$\frac{\partial n}{\partial t} = \frac{\partial^2 n}{\partial x^2} - \alpha H(x)x^2 n, \quad (17)$$

where $\alpha = t_r/P$. Now in astrophysical applications P varies with the crossing time scale in a star cluster, and so α varies nearly as $N/\log N$, where N is the total number of stars (cf. Spitzer 1987). Therefore α can be used nearly as a proxy for N .

In order to estimate an escape rate we adopt the strategy pioneered by Chandrasekhar in this context (Chandrasekhar 1943), which is to look for a separable solution $n(x, t) = \exp(-\lambda t)y(x)$, where we expect $\lambda > 0$. If we impose a no-flux boundary condition at $x = -1$ (say) and the condition that $y(x) \rightarrow 0$ as $x \rightarrow \infty$, then we find that

$$y(x) = \begin{cases} A \cos \left\{ \sqrt{\lambda}(x + 1) \right\} & \text{if } x < 0 \\ B \int_{-\infty}^{-\sqrt{\alpha}} e^{sx^2/2} |\sqrt{\alpha} - s|^{(\lambda/4\sqrt{\alpha} - 3/4)} |\sqrt{\alpha} + s|^{(-\lambda/4\sqrt{\alpha} - 3/4)} ds & \text{if } x > 0, \end{cases} \quad (18)$$

where A, B are constants.

While the first of these solutions is elementary, the second deserves some explanation. As Maple shows, the solution of the differential equation for $y(x)$ when $x > 0$ can be written in terms of Whittaker functions, and a search through Abramowitz & Stegun (1965) shows that these can be expressed as integrals. It is easier, however, to proceed directly, though the appropriate methods are not in common use (cf. Burkill 1962). In this particular case, for a reason that will become clear, we first change the independent variable to $z = x^2/2$. Then the differential equation becomes

$$2z\ddot{y} + \dot{y} + (\lambda - 2\alpha z)y = 0, \quad (19)$$

where a dot denotes a z -derivative. Now we get down to business. Motivated by the inversion integral for Laplace transforms, we seek a solution in the form $y(z) = \int_C \exp(sz)f(s)ds$, where both the function f and the contour C are to be chosen. Substituting into eq.(19), we find that we require

$$\int_C \exp(sz)f(s)(2zs^2 + s + \lambda - 2\alpha z)ds = 0.$$

No non-trivial choice of f will make the integrand vanish. We can, however, integrate by parts to remove the z -dependent part of the last factor of the integrand. It follows that we require

$$[2 \exp(sz) f(s)(s^2 - \alpha)] + \int_C \exp(sz) \left(f(s)(s + \lambda) - \frac{d}{ds} \{2f(s)(s^2 - \alpha)\} \right) ds = 0,$$

where the first term is the end-point contribution. Now the integral can be made to vanish by making the integrand vanish, which in turn requires the solution of a separable first-order differential equation. (Without the precaution of changing from x to z , this would have been a second-order equation.) This gives the integrand in eq.(18b). To make the end-point contribution vanish, we note that we require a function $y(z)$ vanishing as $z \rightarrow \infty$, and the exponential factor in the integrand has this behaviour if we restrict the contour to $\text{Re } s < 0$. One obvious choice for end-point is $s = -\infty$. For the other we choose the negative root of $f(s)(s^2 - \alpha)$, i.e. $s = -\sqrt{\alpha}$, which works if $\lambda < 4\sqrt{\alpha}$. In fact the more stringent condition is the integrability of $f(s)$ at this point, which requires $\lambda < \sqrt{\alpha}$.

Now we must match y and y' at $x = 0$. Evaluating the integral at $x = 0$ is straightforward, and the transformation $s = -\sqrt{\alpha}(1 + 2t)$ gives a standard integral for a beta function. In order to evaluate the derivative $y'(0+)$ one cannot simply differentiate the integral and substitute $x = 0$. For one thing the resulting integral diverges as $s \rightarrow -\infty$. This behaviour is killed by the exponential if x is small and positive, and in this case one can approximate the other factors in the integrand by their asymptotic form as $s \rightarrow -\infty$. Again one obtains a standard integral, this time for a gamma function.

In the end one finds that the relation between λ and α is

$$\tan \sqrt{\lambda} = \sqrt{\frac{4\sqrt{\alpha}}{\lambda}} \frac{\Gamma\left(-\frac{\lambda}{4\sqrt{\alpha}} + \frac{3}{4}\right)}{\Gamma\left(-\frac{\lambda}{4\sqrt{\alpha}} + \frac{1}{4}\right)}. \quad (20)$$

As $\lambda/\sqrt{\alpha} \rightarrow 1-$, the gamma function in the denominator tends to infinity, and so $\sqrt{\lambda} \rightarrow 0$. Thus there is an asymptotic regime such that $\alpha \rightarrow 0$ and $\lambda \simeq \sqrt{\alpha}$. If, on the other hand, $\lambda/\sqrt{\alpha} \rightarrow 0+$, it is clear that the right hand side of eq.(20) tends to infinity, and so $\lambda \rightarrow \pi^2/4$. Numerical study shows that there is a single solution which joins these two asymptotic regimes.

In the second asymptotic regime ($\alpha \rightarrow \infty$, i.e. large N), escape is very efficient, and the time scale for loss of mass, $1/\lambda$, is determined by relaxation. Recalling that we have scaled time by the relaxation time, it follows that the time to lose half the mass, say, varies as t_r . In case α is small, however, escape is the bottleneck, and the escape timescale, in units of the relaxation time, increases as N (or α) decreases. In fact in this regime we expect the half mass time to vary nearly as t_r/\sqrt{N} . Since t_r itself varies nearly as N (in the units of Figure 1), we expect a time scale varying as $t_r^{1/2}$.

These results correspond qualitatively to what is observed (Figure 1). It should be stressed, however, that the value of this toy model is *purely* qualitative. When one studies simulations of the evolution of star clusters quantitatively (Baumgardt 2000b, or those in Figure 1) it is found that, in the case of small N , the actual scaling is more like $t_r^{3/4}$.

We now outline Baumgardt's argument which leads to this scaling. We assume that the distribution of escapers (i.e. those with $E > E_c$) is nearly in equilibrium. Then eq.(17) shows that the width of the distribution is $x \sim \alpha^{-1/4}$. (This scaling can also be seen in eq.(18b).) The number of such escapers is proportional to this width, and can be estimated to be of order $N\alpha^{-1/4}$. The escape time scale at this energy is of order $1/(\alpha x^2)$, $\sim \alpha^{-1/2}$, and therefore the rate of escape is of order $N\alpha^{1/4}$. Thus the time scale for losing (say) half the mass is of order $\alpha^{-1/4}$ in units of the relaxation time, i.e. the time scale of mass loss varies almost as $t_r^{3/4}$.

It is the assumption that the distribution of escapers reaches equilibrium which distinguishes this estimate from the toy model discussed previously, but the reason for this difference is not understood.

6 Distribution of Escape Times

The results of the previous section relate to the time scale on which stars escape, and we conclude with some discussion of the actual *distribution* of escape times. This issue has been studied in a fairly wide variety of problems (e.g. those discussed in the book by Wiggins 1992, and Kandrup et al 1999). In some problems the distribution is found to be approximately exponential, and in others it is better approximated by a power law. For escape in Hill's problem, the numerical experiments summarised in Section 5.3 show that the distribution is approximately a power law, over the range of escape times that are relevant in applications and amenable to numerical study (Fukushige & Heggie 2000).

In this section we shall not even come close to obtaining the distribution of escape times numerically. We shall, however, introduce two tools which show us how to think about this problem. One is a suitable theoretical framework (called *turnstile dynamics*), and the other is a toy model (Hénon 1988) which serves two purposes: (i) it can be used to illustrate turnstile dynamics, and (ii) it was inspired by Hill's problem.

6.1 Hénon's Toy Model

We already presented a surface of section for Hill's problem, and Hénon's model could have been devised with the properties of the corresponding Poincaré map in mind. Physically, however, it can be thought of as the problem of a ball falling under gravity and bouncing off two disks (Figure 8).

When the radius of the disks is very large, Hénon showed that the relation between conditions at each bounce takes a particularly simple form, which is

$$\begin{aligned} X_{j+1} &= X_j \cosh \psi + w_j \sinh \psi - s_j (\cosh \psi - 1) \\ w_{j+1} &= X_j \sinh \psi + w_j \cosh \psi - (s_j \cosh \psi + s_{j+1}) \tanh \frac{\psi}{2}, \end{aligned}$$

where ψ is a parameter (related to the radius of disks, the strength of gravity, etc.), X_j is the x -coordinate at the j th bounce, w_j is the tangential velocity component at this time, and $s_j = \text{sign}X_j$. (There is a tiny subtlety at $X_j = 0$, which we ignore in this exposition.)

The only non-linearities in this problem are the terms with s 's. Otherwise the map is just a hyperbolic rotation about the point $X = \pm 1$, $w = 0$, in the left and right halves of

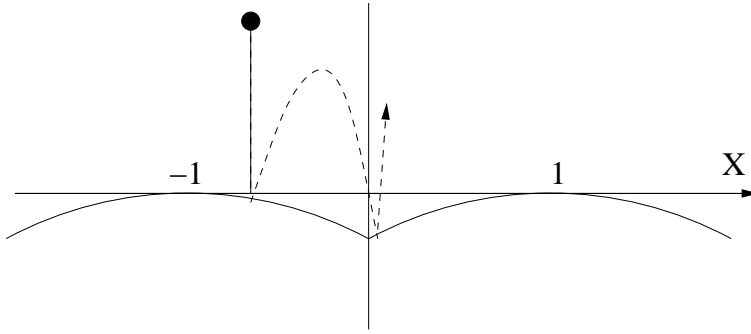


Figure 8. Hénon's billiard model for Hill's problem.

the X, w plane, as appropriate. It is only when a point moves from one half to the other (across the discontinuity in the surface off which the ball bounces) that anything different happens.

These two points are fixed points of the map. As usual in such situations, a fixed point corresponds to a periodic motion, which here refers to the ball bouncing repeatedly off either of the highest points of the disks (Figure 8). These motions are obviously unstable, and the fixed points on the surface of section have local stable and unstable invariant manifolds which are segments of the lines $X = \pm 1 \pm w$ (Figure 9).

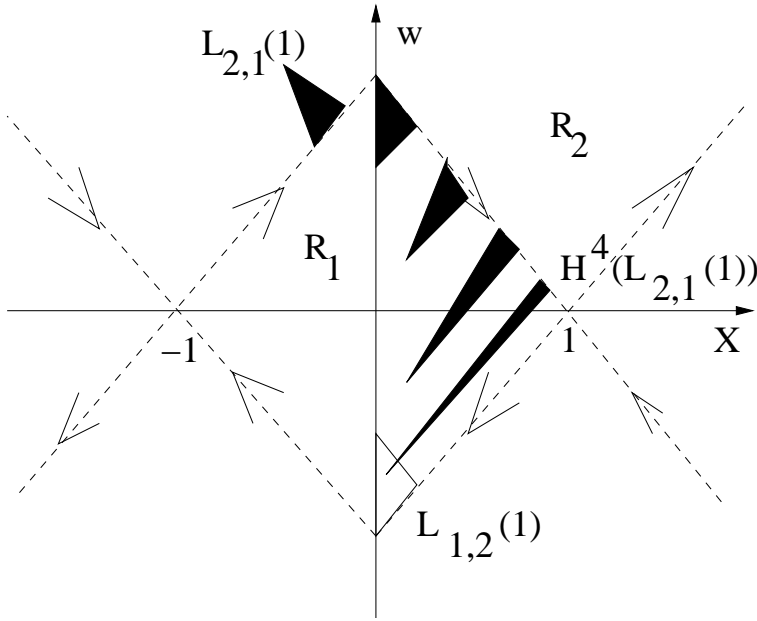


Figure 9. Schematic surface of section for Hénon's model. The dashed lines are the local stable and unstable invariant manifolds of the fixed points at $(\pm 1, 0)$.

What has this to do with Hill's problem? For one thing the unstable periodic orbits have an analogy (in Hill's problem) with the Liapounov orbits mentioned in Sec.5.1. Using the linearised equations derived there it is also possible to derive equations for the local stable and unstable invariant manifolds of the corresponding fixed points on the surface of section (Figure 10). The main difference between the two models is the absence, in Hénon's model, of anything comparable with a limiting curve.

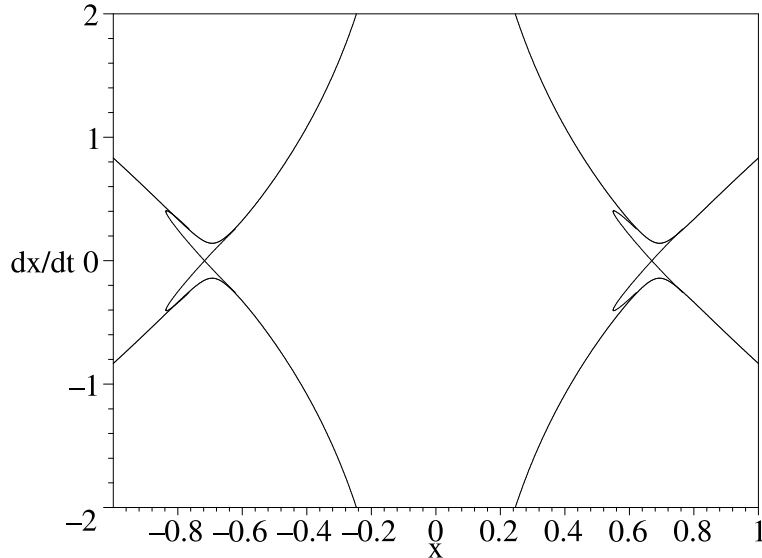


Figure 10. Outline surface of section for Hill's problem, at some energy E just above E_c . The small elliptic arcs are the local stable and unstable manifolds of the fixed points corresponding to the Liapounov orbits, and the large curves are the limiting curves.

6.2 Turnstile Dynamics

In Figure 10 it is fairly obvious how to define the part of the section “inside” the cluster, and how to define the part outside. In Figure 9, despite the absence of limiting curves, we shall define the inside and the outside by the naive resemblance of the two pictures. To be more precise, the inside (R_1) will be defined as the rhombus lying within the stable manifolds of the fixed points, and the outside (R_2) as everything else (Figure 9). This at least makes clear that the boundary between the two regions is to be defined by pieces of the stable and unstable manifolds. This is one of the main procedural points in the theory of turnstile dynamics (Wiggins 1992), which we now introduce via this example. In order to apply this theory to Hill's problem, there also we would have to define the inside and the outside a little more carefully near the fixed points, though we shall not dwell on the details here.

The problem of escape in Hénon's model now focuses on the parts of the surface of section which, under the Poincaré map, are exchanged between regions R_1 and R_2 . A direct calculation (Roy 2000) shows that the region which, on one iteration of Hénon's map, leaves the region R_1 consists of the union of two triangles. One of these is shown on Figure 9 and labelled $L_{1,2}(1)$. The notation, which comes from Wiggins (1992), indicates that this region is a *lobe*, which moves from region R_1 to region R_2 on one iteration. In the usual situation considered by Wiggins, a lobe is bounded by parts of the stable and unstable manifolds of fixed points. This is only partly true in Hénon's model. Two parts of the boundary of the little triangle on Figure 9 have this property: the lower right, which is part of the unstable manifold of the right-hand fixed point, and the boundary at upper right, which consists of part of the stable manifold of the left-hand point. The discontinuity at $X = 0$ provides the remaining part of the boundary.

We now consider capture of phase space from the region R_2 into the region R_1 . Again we have two triangular regions, one of which is shown in Figure 9, and labelled $L_{2,1}(1)$,

as the reader should by now appreciate. Also shown in the Figure are successive iterates of this lobe under the Hénon map H . It can be seen that these remain inside R_1 until the map is iterated 5 times. The region $H^4(L_{2,1}(1))$, which is the black triangle furthest to the lower right, intersects $L_{1,2}(1)$, and after one further iteration this intersection leaves region R_1 (and does so forever, actually. The number of iterations that elapse before such an intersection takes place depends on the value of ψ , of course.)

Now we can see how the distribution of escape times can be analysed, at least in principle. Imagine that, at $t = 0$ (where t counts the number of iterations) the region R_1 is filled uniformly with points. At time $t = 1$, the area occupied by $L_{1,2}(1)$ escapes. The same happens at times $t = 2, 3$, and 4 . At time 5 , however, the number of points that escape is given by the area of $L_{1,2}(1) \setminus H^4(L_{2,1}(1))$. At time 6 the area is now $L_{1,2}(1) \setminus (H^4(L_{2,1}(1)) \cup H^5(L_{2,1}(1)))$, and so on.

Hénon's toy problem is unusual in that some of these calculations can be carried out by elementary means. In almost all problems, by contrast, the work is necessarily numerical. Nevertheless the ideas of turnstile dynamics help to economise the work. The naive way of computing a distribution of escape times, as in Sec.5.3, is to distribute points throughout region R_1 and measure how long they take to escape. We now see, however, that we only need to consider the dynamics of points within $L_{1,2}(1)$ in order to reach the same results. This concentrates the numerical work where it is actually needed.

When we apply these notions to Hill's problem, a number of additional complicating factors arise. In the first place the area on the surface of section is not proportional to the volume of phase space (Binney et al 1985), and therefore does not yield an appropriate measure of the escape rate. Secondly, not all escapers from the Hill potential actually intersect the obvious surface of section $y = 0$. Thirdly, the problem is three-dimensional, and the visualisation of turnstile dynamics becomes harder; Wiggins' book shows some of the complications that arise.

On the other hand, in the planar Hill problem some results are possible. In particular, the analogues of the escape and capture lobes, $L_{1,2}(1)$ and $L_{2,1}(1)$, and their iterates have been mapped out at one or two values of the energy (Roy 2000, Simó & Stuchi 2000). For small numbers of iterations one obtains fairly simple ovals on the surface of section. These are the intersections of the surface of section with the stable and unstable invariant manifolds of the Liapounov orbits, i.e. structures like the tube in Figure 6. For higher numbers of iterations their structure becomes highly convoluted, and further complicated by the fact that, at some intersections, only part of the tube actually intersects the surface.

Another factor which turnstile dynamics clarifies is the relationship between *escape*, which is our interest here, and *temporary capture*, which has motivated other studies (e.g. Murison 1989).

7 Acknowledgements

I thank J. Waldvogel, T. Quinn and C. Simó for interesting conversations about the issues in these lectures, and B. Chauvineau and F. Mignard for a copy of their 1991 publication. Research with H. Baumgardt is supported by PPARC under grant PPA/G/S/1998/00044.

References

- [1] Abramowitz M and Stegun I A, 1965. *Handbook of Mathematical Functions* (New York: Dover)
- [2] Ambartsumian V A, 1938. (“On the dynamics of open clusters”), *Uch. Zap. L.G.U.*, No.22, p.19; translated in eds J Goodman and P Hut *Dynamics of Star Clusters*, Proc. IAU Symp. 113, 521–524 (Dordrecht: Reidel)
- [3] Baumgardt H, 2000a. In *Dynamics of Star Clusters and the Milky Way*, eds S Deiters, B Fuchs, A Just, R Spurzem and R Wielen, in press (San Francisco: ASP)
- [4] Baumgardt H, 2000b. Scaling of N -body calculations, *MNRAS*, submitted
- [5] Benest D, 1971. Elliptic restricted problem for sun-jupiter: existence of stable retrograde satellites at large distance, *A&A* **13** 157–160
- [6] Binney J, Gerhard O E and Hut P, 1985. Structure of surfaces of section *MNRAS* **215** 59–65
- [7] Binney J and Tremaine S, 1987. *Galactic Dynamics* (Princeton: Princeton Univ. Press)
- [8] Burkill J C, 1962. *The Theory of Ordinary Differential Equations* (Edinburgh: Oliver & Boyd)
- [9] Chandrasekhar S, 1942. *Principles of Stellar Dynamics* (Chicago: Univ. of Chicago Press; also New York: Dover, 1960)
- [10] Chandrasekhar S, 1943. Dynamical friction II. The rate of escape of stars from clusters and the evidence for the operation of dynamical friction, *ApJ* **97** 263–273
- [11] Chauvineau B and Mignard F, 1990. Dynamics of binary asteroids. I - Hill's case *Icar* **83** 360–381
- [12] Chauvineau B and Mignard F, 1991. *Atlas of the Circular Planar Hill's Problem* (Grasse: Obs. de la Cote d'Azur)
- [13] Fukushige T and Heggie D C, 2000. The time scale of escape from star clusters *MNRAS* in press
- [14] Gunn J E and Griffin R F, 1979. Dynamical studies of globular clusters based on photo-electric radial velocities of individual stars. I - M3 *AJ* **84** 752–773
- [15] Hénon M, 1969. Numerical exploration of the restricted problem. V. Hill's case: periodic orbits and their stability *A&A* **1** 223–238
- [16] Hénon M, 1988. Chaotic scattering modelled by an inclined billiard *Physica D* **33** 132–156
- [17] Jackson J, 1913. Retrograde satellite orbits *MNRAS* **74** 62–82
- [18] Kandrup H E, Siopis C, Contopoulos G and Dvorak R, 1999. Diffusion and scaling in escapes from two-degree-of-freedom Hamiltonian systems *astro-ph/9904046*
- [19] Leon S, Meylan G and Combes F, 2000. Tidal tails around 20 Galactic globular clusters. Observational evidence for gravitational disk/bulge shocking *A&A* **359** 907–931
- [20] MacKay R S, 1990. Flux over a saddle *Phys. Lett. A* **145** 425–427
- [21] Makino J and Aarseth S J, 1992. On a Hermite integrator with Ahmad-Cohen scheme for gravitational many-body problems *PASJ* **44** 141–51
- [22] Marchal C, 1990. *The Three-Body Problem* (Amsterdam: Elsevier)
- [23] Markellos V V, 2000. *private communication*
- [24] Meylan G, Dubath P and Mayor M, 1991. Two high-velocity stars shot out from the core of the globular cluster 47 Tucanae *ApJ* **383** 587–593

- [25] Moser J K, 1968. Lectures on Hamiltonian Systems *Mem. AMS* **81** 1–60; also in eds R S MacKay and J.D. Meiss, 1987. *Hamiltonian Dynamical Systems* (Bristol: Adam Hilger)
- [26] Murison M A, 1989. The fractal dynamics of satellite capture in the circular restricted three-body problem *AJ* **98**, 2346–59 and 2383–6
- [27] Murray C D and Dermott S F, 1999. *Solar System Dynamics* (Cambridge: Cambridge Univ. Press)
- [28] Oh K S, Lin D N C and Aarseth S J, 1992. Tidal evolution of globular clusters. I. Method *ApJ* **386** 506–18
- [29] Plummer H C, 1918. *An Introductory Treatise on Dynamical Astronomy* (Cambridge: Cambridge Univ. Press; also New York: Dover, 1960)
- [30] Ross D J, Mennim A and Heggie D C, 1997. Escape from a tidally limited star cluster *MNRAS* **284** 811–814
- [31] Roy A, 2000. PhD Thesis, Univ. of Edinburgh, in preparation
- [32] Simó C and Stuchi T J, 2000. Central stable/unstable manifolds and the destruction of KAM tori in the planar Hill problem *Physica D*, **140**, 1–32
- [33] Spitzer L, Jr, 1987. *Dynamical Evolution of Globular Clusters* (Princeton: Princeton Univ. Press)
- [34] Szebehely V, 1967. *Theory of Orbits* (New York: Academic Press)
- [35] Wiggins S, 1992. *Chaotic Transport in Dynamical Systems* (Berlin: Springer-Verlag)